selected with temperatures of 850°C, 875°C, and 900°C, which is cofiring compatible temperature for Ag and low temperature cofired ceramics (LTCC) substrate. Density in different sintering temperature is shown in Figure 2.

Figure 3 shows the XRD patterns of the samples sintered 900°C for 2h in PZT-PZN-PNN based compositions + x wt% CuO ceramics It can be seen in Figure 3 that all samples exhibit a perovskite structure, and that there is no secondary phase until x=0.2 (any peak for secondary phase was not detected in the range of 0.0-0.2). When x was over 0.3, second phase peak was observed, however, a composition for the second peak was not clearly identified.

Figure 4 shows the SEM images of the PZT-PZN-PNN based compositions + x wt% CuO ceramics sintered at 900°C for 2h. As the CuO addition amount increased, grain growth happened whereas small grains disappeared. This grain growth with CuO addition can be explained with liquid phase sintering. Previously, we showed that the addition of CuO can reduce the sintering temperature of the $Pb(Zr,Ti)O_3$-$Pb(Ni,Nb)O_3$ system by the formation of a liquid phase [13]. Thus this liquid phase formation can also be an explanation for the PZT-PZN-PNN based compositions + x wt% CuO ceramics.

Density, dielectric permittivity ($\varepsilon_{33}^T/\varepsilon_0$), electromechanical coupling factor (k_p), mechanical quality factor (Q_m) and piezoelectric constant (d_{33}) were plotted as a function of the amount of CuO addition in Figure 5. The density was increased with the increase of CuO contents approximately from 6.4 to 7.8 g/cm^3. This improvement of the density might be related to the formation of the liquid phase. Moreover, the variation of piezoelectric and dielectric properties showed similar trend to that of density. Therefore, the improved piezoelectric and dielectric properties, which were observed in the range of $x \geq 0.3$, might be due to the increased density as well as increased grain size shown in Figure 4. This hardening effect that could be confirmed by the enhancement of Q_m value approximately from 600 to 1200 as shown in Figure 5.

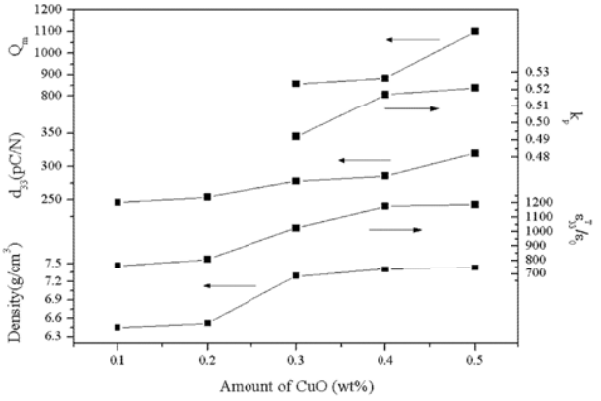

Figure 5. Density, dielectric permittivity ($\varepsilon^T_{33}/\varepsilon_0$), piezoelectric constant (d_{33}), electromechanical coupling factor (k_p) and mechanical quality factor (Q_m) of the specimens sintered at 900°C for 2h in PZT-PZN-PNN based compositions + x wt% CuO ceramics.

Therefore, Cu ions could be expected to enter B site and act as a hardener.

3.2 Effect of Bi_2O_3 Addition

Bi_2O_3 has low melting temperature (817°C) and it was reported that Bi_2O_3 can form liquid phase with ZnO at approximately 750°C. Therefore, Bi_2O_3 was added to PZT-PZN-PNN based compositions + 0.5 wt% CuO in order to further improve the piezoelectric properties of the specimens sintered at low temperature. Density in different sintering temperature is shown in Figure 6.

Figure 7 shows the XRD patterns of the samples sintered 900°C for 2h in PZT-PZN-PNN based compositions + 0.5 wt% CuO + y wt% Bi_2O_3 ceramics. It can be seen that all the samples exhibit a perovskite structure. The base composition (y=0) had a slight tetragonal symmetry. The tetragonality of the peaks was reduced until y=0.3; but it was increased when the amount of Bi_2O_3 addition exceeded 0.3 wt%.

Figure 8 shows the SEM images of the PZT-PZN-PNN based compositions + 0.5 wt% CuO + y wt% Bi_2O_3 ceramics sintered at 900°C for 2 h. When the amount of Bi_2O_3 was more than 0.3 wt%, the small grains almost disappeared and average grain size increased. Even though apparent liquid phase formation was not observed in the SEM images, Bi_2O_3 addition might induce small amount of liquid phase and it could be expected to help grain growth due to its low melting point.

Density, dielectric permittivity ($\varepsilon_{33}^T/\varepsilon_0$), electromechanical coupling factor (k_p), mechanical quality factor (Q_m) and piezoelectric constant (d_{33}) of PZT-PZN-PNN based compositions + 0.5 wt% CuO + y wt% Bi_2O_3 ceramics sintered at 900°C for 2 h are plotted as a function of the amount of Bi_2O_3 addition

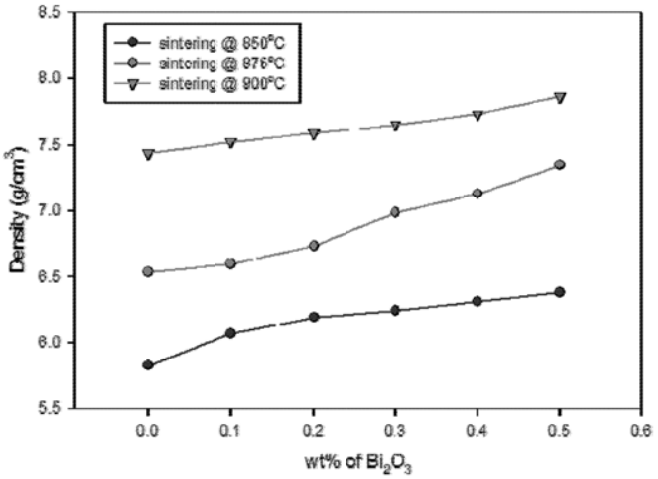

Figure 6. Density in different sintering temperature in PZT-PZN-PNN based compositions + 0.5 wt% CuO + y wt% Bi_2O_3 ceramics.

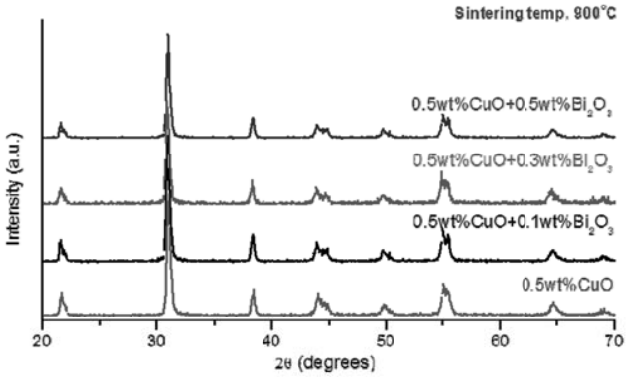

Figure 7. XRD patterns of the samples sintered 900°C for 2h in PZT-PZN-PNN based compositions + 0.5 wt% CuO + y wt% Bi_2O_3 ceramics.

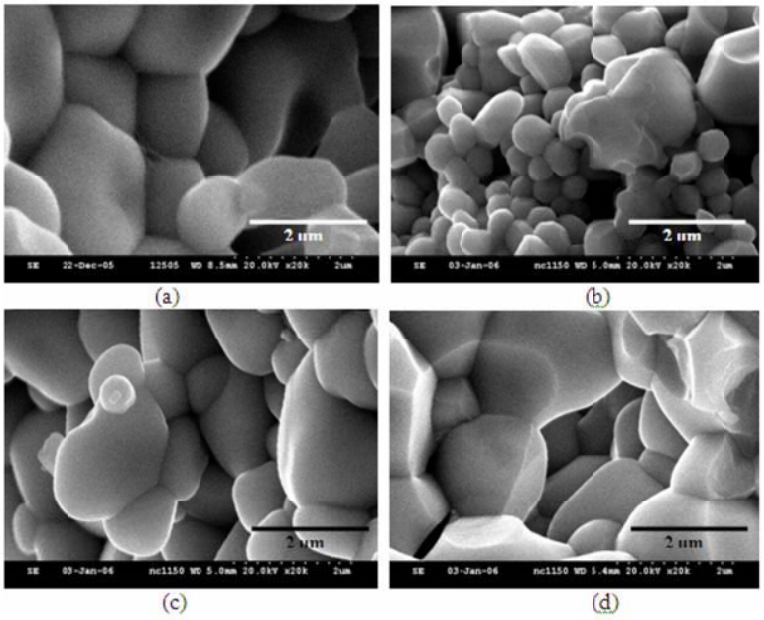

Figure 8. SEM images of the samples sintered at 900°C for 2h in PZT-PZN-PNN based compositions + 0.5 wt% CuO + y wt% Bi_2O_3 ceramics : (a) y=0, (b) y=0.1, (c) y=0.3 and (d) y=0.5.

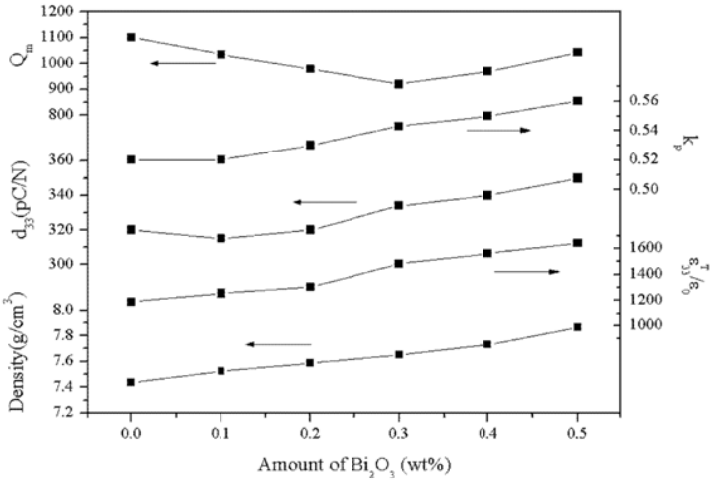

Figure 9. Density, dielectric permittivity ($\varepsilon^{T}_{33}/\varepsilon_0$), piezoelectric constant (d_{33}), electromechanical coupling factor (k_p) and mechanical quality factor (Q_m) of the specimens sintered at 900°C for 2h in PZT-PZN-PNN based compositions + 0.5 wt% CuO + y wt% Bi_2O_3 ceramics.

in Figure 9. When Bi_2O_3 was added, density was increased and this increased density improved the dielectric and piezoelectric properties as seen in Figure 8. The density of the specimens was improved when the amount of Bi_2O_3 was added and this increase might be due to the formation of liquid phase. In addition, Q_m was decreased and $\varepsilon_{33}^{T}/\varepsilon_0$ and d_{33} were increased with the amount of Bi_2O_3 addition in the range of $0.0 \le y \le 0.3$. Therefore, their variations could happen because Bi ions entered A site, since they acted as softener in this range. On the contrary, Q_m exhibits a minimum profile at 0.3 wt% of Bi_2O_3 addition. In addition, $\varepsilon_{33}^{T}/\varepsilon_0$, d_{33} and Q_m were increased with the amount of Bi_2O_3 addition above 0.3 wt%. Thus, Bi ions might act as both hardener and softener in this range and their variations might be able to occur because Bi ions entered B site and A site, respectively.

4. CONCLUSIONS

The addition of CuO decreases the sintering temperature through the formation of a liquid phase. However, the piezoelectric properties of the CuO-added ceramics sintered at below 900°C are lower than the desired values. The additional Bi_2O_3 results in a significant improvement in the piezoelectric properties. Furthermore, at the sintering temperature of 900°C, the electromechanical coupling factor (k_p) , piezoelectric constant (d_{33}), mechanical qulity factor (Q_m) of PZT-PZN based composition ceramics with 0.5 wt% CuO and 0.5 wt% Bi_2O_3 show the optimal value of 0.56, 350 pC/N and 1042, respectively.

5. ACKNOWLEDGEMENTS

This work was supported by the Synchrotron Light Research Institute (Public Organization) SLRI, the Thailand Research Fund (TRF), the Commission on Higher

Education (CHE), and the Faculty of Science, Chiang Mai University. Thank are also extended to Kenji Uchino, ICAT, Penn State for helpful discussion and use of facility during a visit.

REFERENCES

[1] Uchino K., and Giniewicz J.R., *Micromechatronics*, Marcel Dekker, New York, 2003.

[2] Takahashi S., Sintering $Pb(Zr,Ti)O_3$ Ceramics at Low Temperature, *Jpn. J. Appl. Phys.*, 1980; **19**: 771–771.

[3] Lucuta P.G., Constantinescu F., and Barb D., Structural Dependence on Sintering Temperature of Lead Zirconate-Titanate Solid Solutions, *J. Am. Ceram. Soc.*, 1985; **68**: 533-537.

[4] Zhilun G., Longtu L., Suhua G., and Xiaowen Z., Low-Temperature Sintering of Lead-Based Piezoelectric Ceramics, *J. Am. Ceram. Soc.*, 1989; **72**: 486-491.

[5] Patel N.D., and Nicholson P.S., Comparison of piezoelectric properties of hot-pressed and sintered PZT, *Am. Ceram. Soc. Bull.*, 1986; **65**: 783-787.

[6] Yamamoto T., Optimum Preparation Methods for Piezoelectric Ceramics and Their Evaluation, *Am. Ceram. Soc. Bull.*, 1992; **71**: 978-985.

[7] Kaneko S., Dong D., and Murakami K., Effect of Simultaneous Addition of $BiFeO_3$ and $Ba(Cu_{0.5}W_{0.5})O_3$ on Lowering of Sintering Temperature of $Pb(Zr,Ti)O_3$ Ceramics, *J. Am. Ceram. Soc.*, 1998; **68**: 1013-1018.

[8] Wang X., Murakami K., and Kaneko S., High-Performance $PbZn_{1/3}Sb_{2/3}O_3$–$PbNi_{1/2}Te_{1/2}O_3$–$PbZrO_3$–$PbTiO_3$ Ceramics Sintered at a Low Temperature with the Aid of Complex Additives Li_2CO_3–Bi_2O_3–$CdCO_3$, *Jpn. J. Appl. Phys.*, 2000; **39**: 5556–5559.

[9] Hayashi T., Inoue T., and Akiyama Y., Low-Temperature Sintering and Properties of (Pb, Ba, Sr)(Zr, Ti, Sb)O_3 Piezoelectric Ceramics Using Sintering Aids, *Jpn. J. Appl. Phys.*, 1999; **38**: 5547–5552.

[10] Wu L., and Wang C.H., The Dielectric and Piezoelectric Properties of 0.125PMN-0.875PZT Ceramics Doped with $4PbO{\cdot}B_2O_3$, *Jpn. J. Appl. Phys.*, 1999; **32**: 2757–2761.

[11] Wittmer D.E., and Buchanan R.C., Low Temperature Densification of Lead Zirconate Titanate with Vanadium Pentoxide Additive, *J. Am. Ceram. Soc.*, 1981; **64**: 485-490.

[12] Park S. –H., Ural S., Ahn C. –W, Nahm S., and Uchino K., Piezoelectric Properties of Sb-, Li-, and Mn-substituted $Pb(Zr_xTi_{1-x})O_3$–$Pb(Zn_{1/3}Nb_{2/3})O_3$–$Pb(Ni_{1/3}Nb_{2/3})O_3$ Ceramics for High-Power Applications, *Jpn. J. Appl. Phys.*, 2006; **45**: 2667–2673.

[13] Ahn C. –W.,. Song H. –C., and Nahm S., Priya S., Park S. –H, Uchino K., Lee H. –G., and Lee H. –J., Effect of ZnO and CuO on the Sintering Temperature and Piezoelectric Properties of a Hard Piezoelectric Ceramic, *J. Am. Ceram. Soc.*, 2006; **89**: 921-925.

Chiang Mai J. Sci. 2009; 36(1) : 59-68
www.science.cmu.ac.th/journal-science/josci.html
Contributed Paper

Effect of MnO_2 Addition on Dielectric, Piezoelectric and Ferroelectric Properties of $0.2Pb(Zn_{1/3}Nb_{2/3})O_3$–$0.8Pb(Zr_{1/2}Ti_{1/2})O_3$ Ceramics

Athipong Ngamjarurojana, and Supon Ananta*
Department of Physics, Faculty of Science, Chiang Mai University, Chiang Mai 50200, Thailand.
*Author for correspondence; e-mail: suponananta@yahoo.com

Received: 20 December 2008
Accepted: 7 January 2009.

Abstract

Piezoelectric materials are presently being extensively developed for applications such as ultrasonic motors and piezoelectric transformers. In this study, the dielectric, piezoelectric, and ferroelectric properties of MnO_2-doped $0.2Pb(Zn_{1/3}Nb_{2/3})O_3$-$0.8Pb(Zr_{1/2}Ti_{1/2})O_3$ (hereafter 0.2PZN-0.8PZT), which is the morphotropic phase boundary composition of the PZN-PZT system, were investigated. It was found that crystal structure moved to rhombohedral side when increasing MnO_2 content. With the addition of MnO_2, Curie temperature T_c, the piezoelectric constant d_{33}, and electromechanical coupling factor k_p were slightly decreased, but the mechanical quality factor Q_m was significantly increased. The P–E and s-E loop demonstrated decreased P_r and strain level but increased E_c with addition of MnO_2. These results clearly showed the significance of MnO_2 addition on the electrical properties of the PZN–PZT system with "hard" characteristics.

Keywords: dielectric, piezoelectric, ferroelectric, hard doping.

1. Introduction

All commercial piezoelectric devices employ $Pb(Zr,Ti)O_3$ (PZT)-based formulations, close to the morphotropic phase boundary (MPB). The MPB composition is modified by the acceptor and/or donor ions to yield high piezoelectric properties with low losses. The influence of various substitutions on the B-site of $Pb(Zr,Ti)O_3$ perovskite has been widely investigated to optimize the piezoelectric properties [1-6]. Fan and Kim [7] investigated $Pb(Zn_{1/3}Nb_{2/3})_{0.5}(Zr_{0.47}Ti_{0.53})_{0.5}O_3$ ceramics with composition close to MPB and clarified that the ceramics had large electro-mechanical coupling factor k_p. However, the mechanical quality factor Q_m was too low to permit their use as high power piezoelectric devices. It is necessary to improve Q_m as much as possible for suppressing the generation of heat during operation. To develop materials suitable for multilayer piezoelectric transformers and actuators with high d_{33}, high k_p and Q_m, it is necessary to add some dopants to PZN–PZT based ceramics to optimize the piezoelectric properties for device applications [8-11].

Manganese ions have been investigated extensively as effective dopant in PZT-based ceramics because Mn ions can have valence

3. RESULTS AND DISCUSSION

Perovskite phase formation, crystal structure and lattice parameter were determined by XRD at room temperature. The XRD patterns of $0.2Pb(Zn_{1/3}Nb_{2/3})O_3$-$0.8Pb(Zr_{1/2}Ti_{1/2})O_3$, with the addition of 0.0-0.9 wt% MnO_2 are shown in Figure 1, showing the perovskite structure for all compositions. The pyrochlore phase is not observed in this system. In the XRD patterns, the crystal structure of the specimens appears clearly to change to rhombohedral side across MPB with increasing amount of MnO_2 around 0.5 wt%. It has been reported [6,8] that manganese coexists mainly in the Mn^{2+} and Mn^{3+} states, which entered into the perovskite structure of BO_6 octahedron to substitute for the B-site ion (e.g., Ti^{4+} and Zr^{4+}).

Figure 2 shows SEM photographs of the surfaces of $0.2Pb(Zn_{1/3}Nb_{2/3})O_3$-$0.8Pb(Zr_{1/2}Ti_{1/2})O_3$ ceramics doped with 0.0–0.9 wt% MnO_2. As shown in Figs. 2(a-b), the grain sizes of the ceramics are increased with increasing amount of MnO_2 addition. The result is similar to the result of Yu *et al.* [16]. Further increasing MnO_2 content gives rise to an inhomogeneous grain size. However, the SEM micrographs in Figure 2(c-f) show that a higher porosity level is observed when the amount of MnO_2 is increased [17]. The above results are obviously consistent with the change in the bulk density with MnO_2 content for Mn-doped $0.2Pb(Zn_{1/3}Nb_{2/3})O_3$-$0.8Pb(Zr_{1/2}Ti_{1/2})O_3$ ceramics. It can clearly be seen from Figure 2 that the ceramics have high densities in the MnO_2 addition range of 0.0-0.5 wt%. It is believed that manganese ions are mainly incorporated into the lattice, but if the addition is above 0.5 wt%, manganese ions will accumulate at the grain boundaries [14]. These inferences are obviously consistent with the changes mentioned above in the microstructures. The micrographs also show that the grain size of the ceramics varies considerably, as listed in Table 1.

The temperature and frequency dependences of the dielectric constant (ε_r) and dielectric loss tangent (tan δ) for 0.2PZN–0.8PZT + x wt% MnO_2, x = 0, 0.1, 0.3, 0.5, 0.7 and 0.9 are shown in Figure 3. The maximum dielectric constant at 1 kHz (ε_m @ 1 kHz) is listed in Table 2. Dielectric behaviors show strong increase of frequency-dependence on dielectric constant and dielectric loss with increasing amount of MnO_2. It may be caused from oxygen vacancies and conducting regions near grain boundaries [18] when increasing MnO_2. The variation of the Curie temperature (T_c) as a function of composition x is plotted in Figure 4. The Curie temperature of 0.2PZN–0.8PZT + x wt% MnO_2 system can be varied over a wide range

Table 1. Physical properties of 0.2PZN–0.8PZT + x wt% MnO_2 ceramics.

x	Density (g/cm³)	Grain size range(μm)	Average grain size (μm)
0	7.826	0.5 - 2.0	1.726
0.1	7.849	1.5 – 6.0	4.131
0.3	7.897	1.0 – 3.0	2.991
0.5	8.028	0.5 – 2.0	2.116
0.7	7.718	-	-
0.9	7.653	-	-

Table 2. Dielectric and piezoelectric properties of 0.2PZN–0.8PZT + x wt% MnO_2 ceramics.

x	T_C (°C)	Dielectric properties (at 25 °C, 1 kHz)		Dielectric properties (at T_{Max})		Piezoelectric properties		
		ε_r	tanδ	ε_r	tanδ	d_{33}(pC/N)	k_p	Q_m
0	339.7	1575	0.0249	21047	0.0420	430	0.583	90
0.1	334.2	1155	0.0436	17784	0.1181	365	0.564	356
0.3	326.5	1100	0.0464	19102	0.1241	320	0.551	735
0.5	323.4	1086	0.0440	18220	0.1454	305	0.532	1413
0.7	318.7	1020	0.0368	21178	0.1354	263	0.48	1260
0.9	311	948	0.0438	21389	0.1762	237	0.44	1080

Table 3. Ferroelectric and strain properties of 0.2PZN–0.8PZT + x wt% MnO_2 ceramics .

x	Ferroelectric properties (at 25 °C)			Loop squareness (R_{sq})	Strain %@ 4MV/m
	P_r (C/m²)	P_s (C/m²)	E_C (MV/m)		
0	0.287	0.300	1.97	1.483	0.278
0.1	0.224	0.233	2.18	1.488	0.231
0.3	0.208	0.213	2.37	1.712	0.188
0.5	0.147	0.175	1.94	1.024	0.162
0.7	0.089	0.126	1.63	0.811	0.134
0.9	0.077	0.111	1.75	0.811	0.115

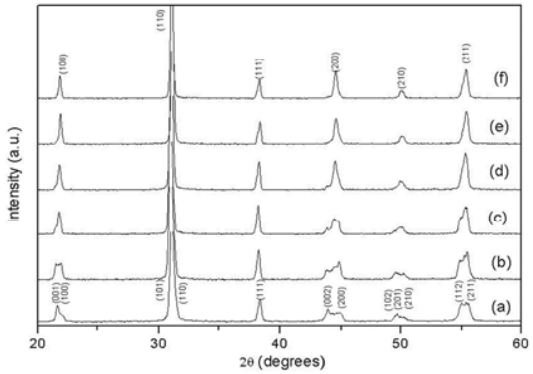

Figure 1. XRD patterns of the samples sintered at 1200°C for 2h of 0.2PZN–0.8PZT + x wt% MnO_2 ceramics: (a) x =0, (b) x =0.1, (c) x =0.3, (d) x =0.5, (e) x =0.7 and (f) x =0.9.

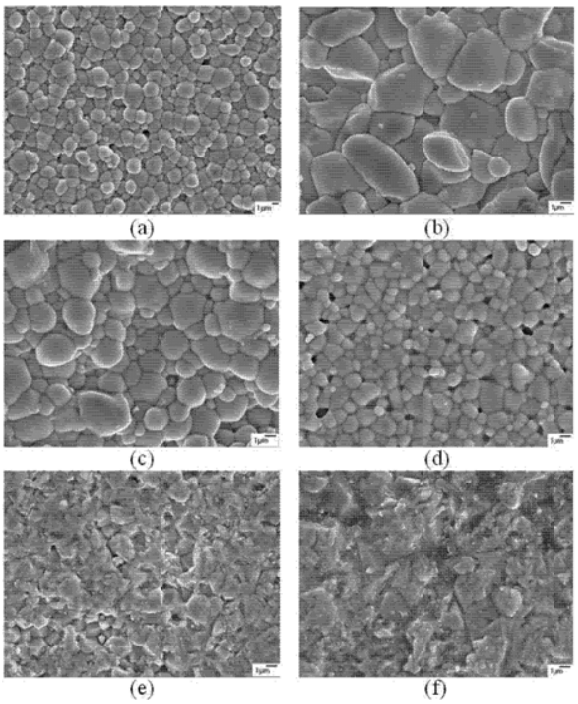

Figure 2. SEM images of the specimens sintered surface of 0.2PZN–0.8PZT + $x$wt% MnO_2 ceramics at 1200°C for 2h; (a) x=0, (b) x=0.1, (c) x=0.3, (d) x=0.5, (e) x=0.7 and (f) x=0.9.

from 310 to 340 °C by controlling the addition of MnO_2 content in the system. The results indicate a rapid decrease in T_c with an increase in MnO_2 content over the range from 0.0 to 0.9 wt%.

Density, dielectric constant (ε_r), electro-mechanical coupling factor (k_p), mechanical quality factor and piezoelectric constant (d_{33}) are plotted as a function of amount of MnO_2 addition in Figure 5. When the amount of MnO_2 is lower than 0.5 wt%, density slightly increases. However, ε_r, k_p and d_{33} show decreasing trends with increasing MnO_2 content. When the amount of MnO_2 is lower than 0.5 wt%, k_p and d_{33} are rapidly decreased with increasing MnO_2 content. It is well known that the substitutions of acceptor dopant Mn ions will lead to the creation of oxygen vacancies, which pin the movement of the ferroelectric domain walls and result in a decrease of ε_r, k_p and d_{33}[11,19]. The mechanical quality factor (Q_m) increases rapidly with increasing MnO_2 content [4]. The acceptor dopant of MnO_2 improves Q_m significantly. The highest value Q_m (~1413) are obtained in the ceramics with MnO_2 amounts of 0.5 wt%. Further addition of MnO_2 above 0.5 wt% leads to a slightly decrease in the value of Q_m, which may be mainly attributable to non-uniformity of the

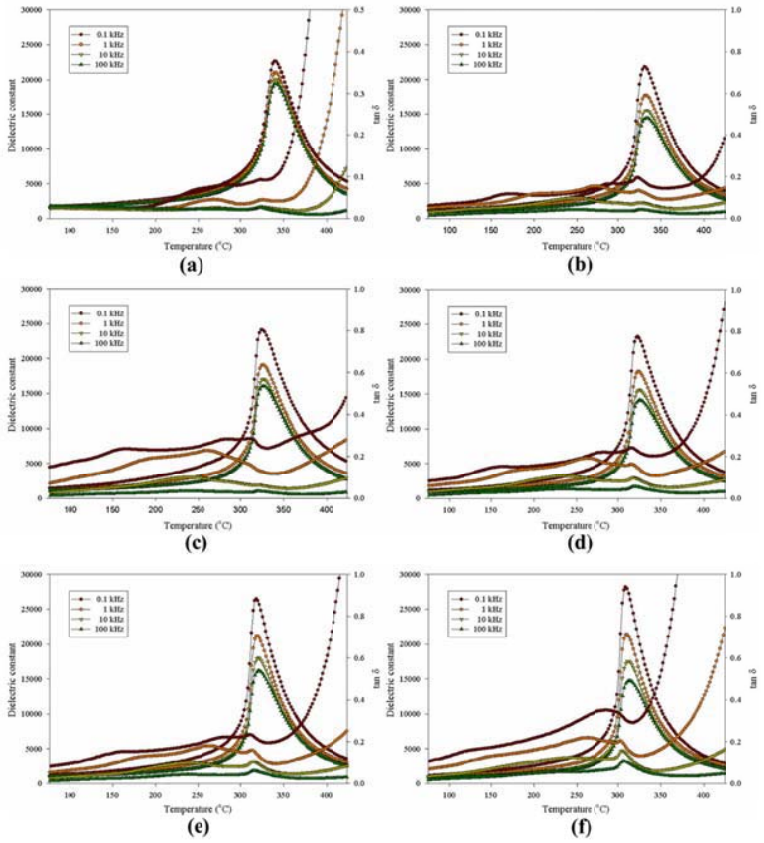

Figure 3. Temperature and frequency dependence of dielectric properties of 0.2PZN–0.8PZT + x wt% MnO_2 ceramics at 1200°C for 2h; (a) x =0, (b) x =0.1, (c) x =0.3, (d) x =0.5, (e) x =0.7 and (f) x =0.9.

microstructure, as shown in Figure 2.

The polarization-field (P–E) hysteresis loops of 0.2PZN–0.8PZT + x wt% MnO_2 ceramics are shown in Figure 6. The well-developed and fairly symmetric hysteresis loops with the field are observed for all compositions. To further assess ferroelectric characteristics in MnO_2-modified PZN-PZT ceramics, the ferroelectric parameters, i.e. the remnant polarization (P_r) and the coercive field (E_c), have been extracted from the experimental data and given in Table 3. It can be seen that P_r and P_s decrease with an addition of MnO_2 into the PZN–PZT

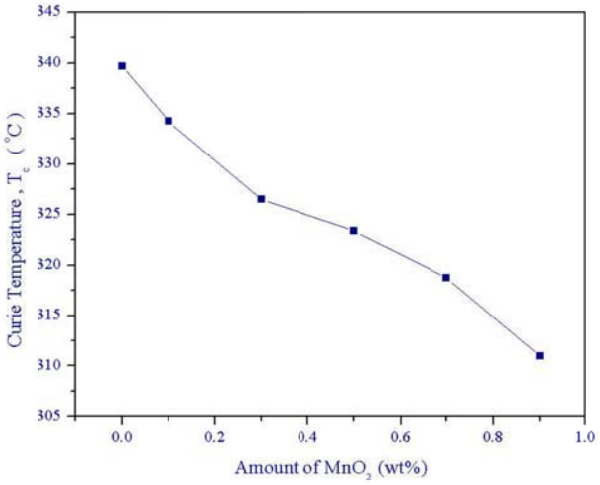

Figure 4. Curie temperature of the specimens sintered at 1200°C for 2h of 0.2PZN–0.8PZ + x wt% MnO_2 ceramics where x = 0 , 0.1 ,0.3 0.5, 0.7 and 0.9.

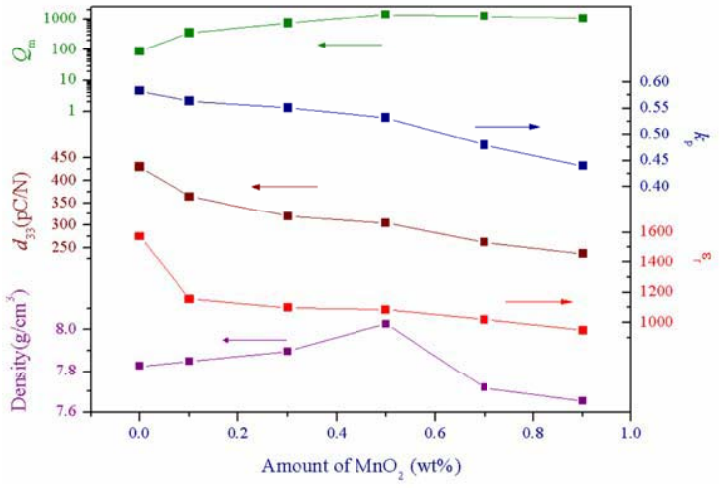

Figure 5. Density, dielectric constant (ε_r), piezoelectric constant (d_{33}), electromechanical coupling factor (k_p), and mechanical quality factor (Q_m) of the specimens sintered at 1200°C for 2h of 0.2PZN–0.8PZT + x wt% MnO_2 ceramics where x = 0 , 0.1 ,0.3, 0.5, 0.7 and 0.9.

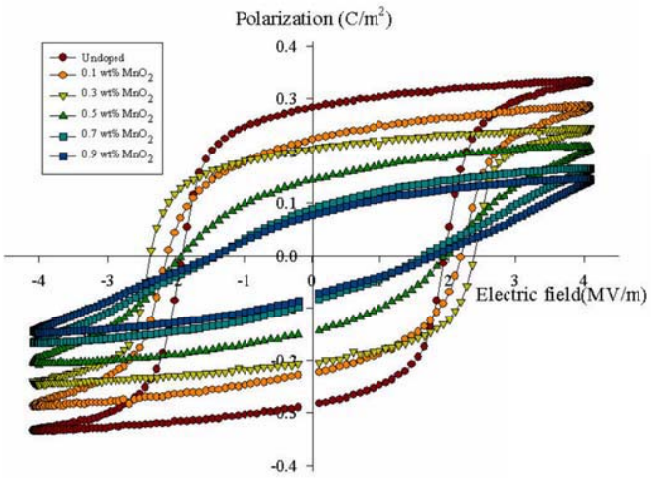

Figure 6. Polarization and electric field (P-E) loops of 0.2PZN–0.8PZT + *x* wt% MnO_2 ceramics.

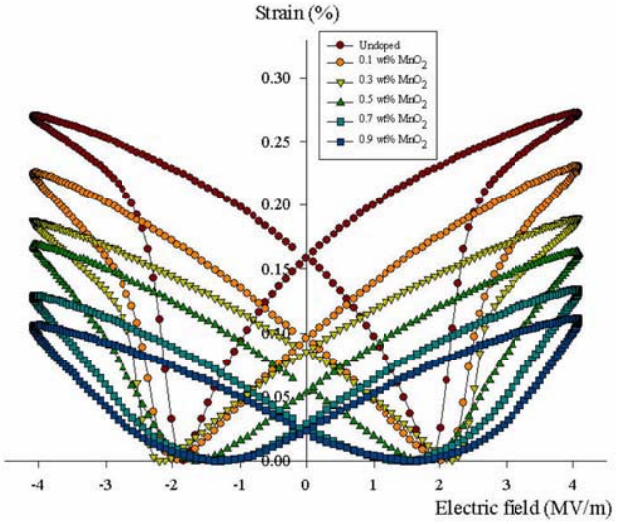

Figure 7. Strain and electric field (s-E) loops of 0.2PZN–0.8PZT + *x* wt% MnO_2 ceramics.

composition, while E_c increases to the maximum at $x = 0.3$ wt%. The ferroelectric characteristics can also be assessed with the hysteresis loop squareness (R_{sq}), which can be calculated from the empirical expression $R_{sq}=(P_r/P_s)+(P_{1.1Ec}/P_s)$, where P_r is the remnant polarization, P_s is the saturated polarization obtained at some finite field strength below the dielectric breakdown and $P_{1.1Ec}$ is the polarization at the field equal to $1.1E_c$ [20]. For the ideal square loop, R_{sq} is equal to 2.00. As listed in Table 3, the R_{sq} parameter increases from 1.483 in $x = 0$ to reach the maximum value of 1.712 in $x = 0.3$. Further addition of MnO_2 above 0.3 wt% leads to a decrease in the R_{sq} parameter, which is mainly attributable to non-uniformity of the microstructure, as shown in Figure 2. The longitudinal strain (s) of the specimens as a function of the electric field is shown in Figure 7. The strains are degraded markedly when MnO_2 content is increased, as listed in Table 3. These results (decreased P_r and strain level but increased E_c) clearly indicate the "hard" characteristics with addition of MnO_2, mainly caused by Mn ions substitution in B-site leads to the creation of oxygen vacancies, which pin the movement of the ferroelectric domain walls.

4. CONCLUSIONS

The structure and electrical properties of MnO_2-doped $0.2Pb(Zn_{1/3}Nb_{2/3})O_3$-$0.8Pb(Zr_{1/2}Ti_{1/2})O_3$ ceramic, which is the MPB composition of the PZN-PZT system, are investigated. The addition of MnO_2 content transforms the crystal structure to rhombohedral side. Furthermore, MnO_2 addition decreases the Curie temperature, ε_r, d_{33} and k_p, but enhances the mechanical quality factor. The P–E and s-E loops demonstrate decreased P_r and strain level with increased E_c with addition of MnO_2. These results clearly show the hardening influence of MnO_2 in the PZN–PZT system.

5. ACKNOWLEDGEMENTS

This work was supported by the Synchrotron Light Research Institute (Public Organization) SLRI, the Thailand Research Fund (TRF), the Commission on Higher Education (CHE), and the Faculty of Science, Chiang Mai University.

REFERENCES

[1] Jin B.M., Kim J., and Kim S.C., Effects of grain size on the electrical properties of $PbZr_{0.52}Ti_{0.48}O_3$ ceramics, *Appl. Phys. A: Mater.*, 1997; **65**: 53-55.

[2] Yudong H., Mankang Z., and Feng G., Effect of MnO_2 Addition on the Structure and Electrical Properties of $Pb(Zn_{1/3}Nb_{2/3})_{0.2}(Zr_{0.50}Ti_{0.50})_{0.80}O_3$ Ceramics, *J. Am. Ceram. Soc.*, 2004; **87**: 847-850.

[3] Vasileva T.K., Nadoliisky M.M., and Toshev S.D., Study of PZT ceramics doped with Cr_2O_3, *Phys. Status Solidi. (a).*, 1984; **86**: 109–111.

[4] Toshio K., Toshimasa S., and Takaaki T., Effects of Manganese Addition on Piezoelectric Properties of $Pb(Zr_{0.5}Ti_{0.5})O_3$, *Jpn. J. Appl. Phys.*, 1992; **31**: 3058–3060.

[5] Takahashi S., and Takahashi M., Effects of Impurities on the Mechanical Quality Factor of Lead Zirconate Titanate Ceramics, *Jpn. J. Appl. Phys.*, 1972; **11**, 31–35.

[6] Kim J.S., Yoon K.H., Choi B.H., Park J.O., and Lee J.M., Effects of MnO_2 on the Dielectric and Piezoelectric Properties of $Pb(Zr_{0.52}Ti_{0.48})O_3$ Ceramics, *J. Kor. Ceram. Soc.*, 1990; **27**: 187-194.

[7] Fan H.Q., and Kim H.E., Effect of Lead Content on the Structure and Electrical Properties of $Pb((Zn_{1/3}Nb_{2/3})_{0.5}(Zr_{0.47}Ti_{0.53})_{0.5})O_3$ Ceramics, *J. Am. Ceram. Soc.*, 2001; **84**: 636-638.

[8] Xu Y., *Ferroelectric Materials and Their Applications*, Elsevier Science Publishers, Amsterdam, The Netherlands, 1991.

[9] Uchino K., Giniewicz J.R., *Micromechatronics*, Marcel Dekker, New York, 2003.

[10] Moulson A.J., and Herbert J.M., *Electroceramics (2nd ed.)*, Wiley, New York, 2003.

[11] Jaffe B., Cook W.R., and Jaffe H., *Piezoelectric Ceramics*, Academic Press Inc., New York, 1971.

[12] Yoo J., Hong J., and Suh S., Effect of MnO_2 impurity on the modified $PbTiO_3$ system ceramics for power supply, *Sens. Actuators*, 1999; **78**: 168-171.

[13] Priya S., Ph.D. Dissertation, Pennsylvania State University, USA., 2003.

[14] He L.X., and Li C.E., Effects of addition of MnO on piezoelectric properties of lead zirconate titanate, *J. Mater. Sci.*, 2000; **35**: 2477-2480.

[15] IEEE Standard on Piezoelectricity, *IEEE Standard* 176–1978, Institute of Electrical and Electronic Engineers, New York, 1978.

[16] Yu C.-S., Hsieh H.-L., X ray investigation of high oriented $(1 - x)PbMg_{1/3}Nb_{2/3}O_3$–$(x)PbTiO_3$ ceramics, *J. Euro Ceram. Soc.*, 2005; **25**: 2435-2427.

[17] Hou Y.D., Cui B., Zhu M.K., Wang H., Wang B., Yan H., Tian C.S., Structure and electrical properties of Mn-modified $Pb((Zn_{1/3}Nb_{2/3})_{0.20}(Zr_{0.50}Ti_{0.50})_{0.80})O_3$ ceramics sintered in a protective powder atmosphere, *Mater. Sci. and Eng. B*, 2004; **111**: 77-81.

[18] Wersing W., Anomalous dielectric losses in manganese doped lead-titanate-zirconate-ceramics, *Ferroelectrics*, 1978; **22**: 813-815.

[19] Wut L., Wei C.-C., Wu T.-S., and Teng C.-C., Improved ceramics for piezoelectric devices, *J. Phys. C: Solid State Phys.*, 1983; **16**: 2813-2821.

[20] Yimnirun R., Ananta S., Ngamjarurojana A., and Wongsaenmai S., Uniaxial stress dependence of ferroelectric properties of x PMN-$(1 - x)$ PZT ceramic systems, *Appl. Phys. A: Mater.*, 2005; **81**: 1227-1231.

Key Engineering Materials Vols. 421-422 (2010) pp 550-553
© (2010) Trans Tech Publications, Switzerland
doi:10.4028/www.scientific.net/KEM.421-422.550

Effect of Vibro- Milling Time on Phase Formation and Particle Size of $ZnNbO_6$ Nano-powders

Athipong Ngamjarurojana[1,*], Rattikorn Yimnirun[2] and Supon Ananta[1]

[1]Department of Physics, Faculty of Science, Chiang Mai University, Chiang Mai 50200 Thailand
[2]School of Physics, Institute of Science, Suranaree University of Technology, Nakhon Ratchasima 30000 Thailand

Keywords: Zinc niobate; Vibro-milling; solid-state reaction; Microstructure; Dielectric Properties

ABSTRACT

Zinc niobate, $ZnNb_2O_6$, nanopowders was synthesized by a solid-state reaction via a rapid vibro-milling technique. The effect of milling time on the phase formation and particle size of $ZnNb_2O_6$ powder was investigated. The formation of the $ZnNb_2O_6$ phase investigated as a function of calcination conditions by DTA and XRD. The particle size distribution of the calcined powders was determined by laser diffraction technique, while morphology, crystal structure and phase composition were determined via a SEM techniques. In addition, by employing an appropriate choice of milling time, a narrow particle size distribution curve was also observed.

INTRODUCTION

Zinc niobate ($ZnNb_2O_6$, ZN) is one of the binary niobate compounds which exhibits excellent dielectric properties at microwave frequencies [1-2]. It has very low loss and high dielectric constant and is a promising candidate for application in microwave devices[3-4]. Moreover, the columbite-structured $ZnNb_2O_6$ is well known as an attractive B-site precursor for the preparation of lead zinc niobate ($Pb(Zn_{1/3}Nb_{2/3})O_3$ or PZN)-based ferroelectric ceramics used for high performance electromechanical actuators and transducers and piezoelectric ultrasonic motors [5-7]. This is significant because it is very difficult to synthesize those compounds via the conventional solid-state reaction process using oxides as starting materials [8-10]. In the past, $ZnNb_2O_6$ powders were usually prepared by a solid-state reaction process [11-13]. Recent work by Vittayakorn *et. al.* [14] has also shown promise in producing pure phase columbite ZN powders with the conventional mixed-oxide ball milling method technique that used very long heat treatments at ~950-1350 °C for 4h, while Ngamjarurojana *et. al.*[15] has successfully synthesized ZN powders via a rapid vibro-milling technique, which have been developed as alternatives to the conventional solid-state reaction of mixed oxides. These techniques are aimed at reducing the temperature of preparation of the compound by mixed oxide route.
Therefore, the main purpose of this work is to explore a simple mixed oxide synthetic route for the production of $ZnNb_2O_6$ (ZN) powders via a rapid vibro-milling technique and to perform milling time, which calcined at 600 °C for 2 h with heating/cooling rates 5 °C/min, on the phase formation and particle size of $ZnNb_2O_6$ powder was investigated.

EXPERIMENTAL

In this study, starting materials were commercially available zinc oxide, ZnO (Fluka Chemical, 99.9% purity) and niobium oxide, Nb_2O_5 (Aldrich, 99.9% purity). $ZnNb_2O_6$ powders were synthesized by the solid-state reaction of these raw materials. Ground mixtures of the powders were required with stoichiometric ratio of ZnO and Nb_2O_5 powders. A McCrone vibro-milling technique

was employed in order to combine mixing capacity with a significant time saving. The milling operation was carried out in isopropanal. High purity corundum cylindrical media were used as the milling media. After varied vibro-milling from 0.5- 25 h. and drying at 120 °C, the mixture was calcined at 600 °C for 2 h with heating/cooling rates 5 °C/min[13] in alumina crucible to investigate the phase formation behavior of ZN powders. Calcined powders were subsequently examined by room temperature X-ray diffraction (XRD; Siemens-D500 diffractrometer) using Ni-filtered CuK_α radiation to identify the phases formed for the ZN powders. Powder morphologies and particle sizes were directly imaged using scanning electron microscopy (SEM; JEOL JSM-840A). The particle size distributions of the powders were determined by laser diffraction technique (Zetasizer Nano; Malvern Particle Size).

RESULTS AND DISCUSSION

All calcined powders in together different vibro-milling time as shown in Fig. 1. It can be noticed that all conditions is pure phase of $ZnNb_2O_6$ which are matched in JCPDS file number 30-0873.

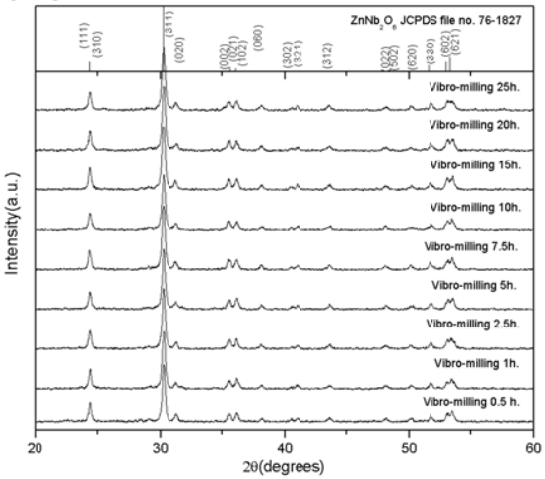

Fig. 1 XRD patterns of the ZN powders calcined at 600 °C for 2 h with heating/cooling rates 5 °C/min with various milling times.

Fig. 2 shows the morphological evolution of all samples as a function of milling times. In general, the particles are agglomerated and basically irregular in shape, with a substantial variation in particle sizes. By increasing the milling time from 0.5 h to 25 h, the particle size of the ZN powder almost similar in size and shape. This is probably due to the effectiveness of vibro-milling and carefully optimized reaction. It is also of interest to point out that larger particle size was obtained for the milling time longer than 10 h. This observation may be attribute to the occurrence of hard agglomeration with strong inter-particle bond within each aggregates resulting from high energy of too long milling time process.

The effect of milling time on particle size distribution was found to be quite significant as shown in Fig 3. After milling times of 0.5–7.5 h, the powders have similar particle size distribution behavior. They exhibit a single peak covering the size ranging from 0.3 – 0.8 μm. By increasing the milling time to 10 h, a uniform particle size distribution with a much lower degree of particle agglomeration was found. However, upon further increasing of milling time up to 25h, a distribution curve with peak broadening between 0.2 – 1 μm was observed. This may be attribute to

the formation of hard and large agglomeration found in the SEM results. In this work, it is seen that the optimum milling time for the production of smallest nanosized and high purity ZN powder was found to be at 10 h. Variations in these data may be attributed mainly to the formation of hard and large agglomerations found in the SEM results.

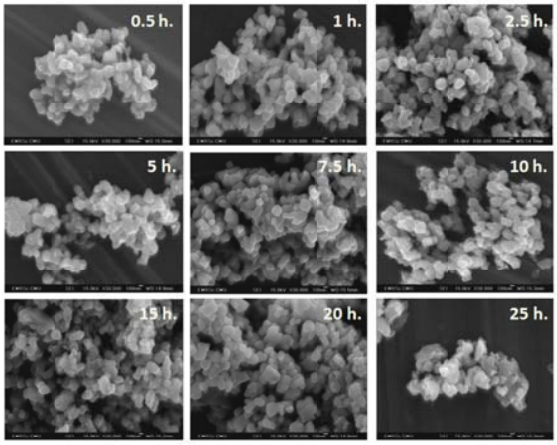

Fig. 2 SEM micrographs of the calcined ZN powders with various milling times.

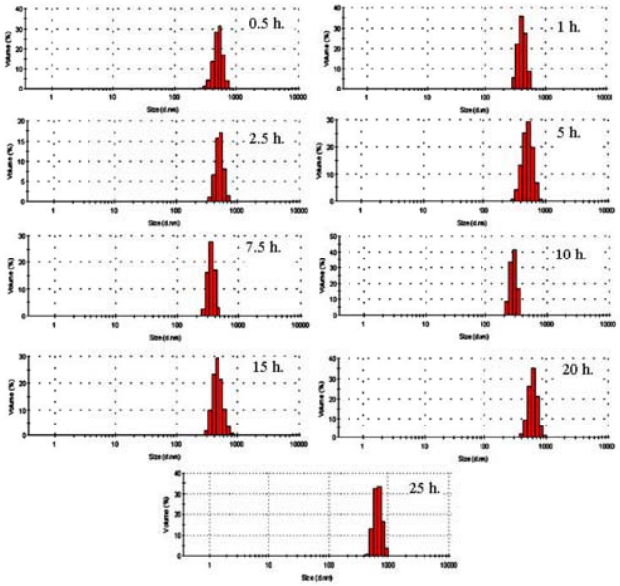

Fig. 3 Particle size distribution curves of the calcined ZN powders with various milling times.

CONCLUSIONS

The effect of milling times on phase formation, particle size and particle size distribution of perovskite zinc niobate synthesized by the solid-state reaction via a rapid vibro-milling technique was investigated. The resulting ZN nano-sized powders consist of a variety of agglomerate particle size, depending on milling times.

ACKNOWLEDGEMENTS

This work was supported by the Thailand Research Fund (TRF), the Commission on Higher Education (CHE) and the Faculty of Science, Chiang Mai University.

REFERENCES

[1] R. C. Pullar, K. Okeneme and N. M. Alford, J. Eur. Ceram. Soc., 23 (2003) 2479.
[2] D.W. Kim, K.H. Ko, K.S. Hong, J. Am. Ceram. Soc. 84 (6) (2001) 1286.
[3] A.Z. Simoes, A.H.M. Gonzalez, A.A. Cavalheiro, M.A. Zaghete, B.D. Stojanovic, J.A. Varela, Ceram. Inter. 28 (2002) 265.
[4] L.J. Hu, Y.H. Chang, I.N. Lin, S.J. Yang, J. Cryst. Growth. 114 (1991) 191.
[5] Xu, Y., *Ferroelectric Materials and Their Applications*. Elsevier Science, Amsterdam, The Netherlands, 1991.
[6] G. Haertling, J. Am. Ceram. Soc. 82 (1999) 797.
[7] A.J. Moulson, J.M. Herbert, Electroceramics, 2nd ed., A Wiley-Interscience, New York, 2004
[8] T.R. Gururaja, A. Safari, A.Halliyal, Am. Ceram. Soc. Bull. 65 (1986) 1601.
[9] M.M.A. Sekar, A. Halliyal, K.C. Patil, J. Mater. Res., 1996, **11**, 1210.
[10] H.J. Lee, K.S. Hong, S.J. Kim, Mater. Res.Bull. 32 (7) (1997) 847.
[11] Y. Hou, M.K. Zhu, H. Wang, B. Wang, H. Yan, C.S. Tian, Mater. Lett. 58 (2004) 1508.
[12] W. Zhu, A.L. Kholkin, P.Q. Mantas, J.L. Baptista, J. Am. Ceram. Soc. 84 (2001) 1740.
[13] M. Villegas, A.C. Caballero, C. Moure, P. Durán, J.F. Fernández, R.E. Newnham, J. Am. Ceram. Soc. 83 (2000) 141.
[14] N. Vittayakorn, G. Rujijanagul, T. Tunkasiri, X. Tan, D.P. Cann, *J. Mater. Res.*,2003, **18**, 2882.
[15] A. Ngamjarurojana, O. Khamman, R. Yimnirun and S. Ananta , Mater. Lett. 60 (2006) 2863

e-mail: ngamjarurojana@yahoo.com

Fax: +66-53-943445

GFER #482888, VOL 405, ISS 1

Extended X-Ray Absorption Fine Structure and X-Ray Diffraction Studies of Mn-Doped PZN-PZT Ceramics

Athipong Ngamjarurojana, Laongnuan Srisombat, Rattikorn Yimnirun, and Supon Ananta

QUERY SHEET

This page lists questions we have about your paper. The numbers displayed at left can be found in the text of the paper for reference. In addition, please review your paper as a whole for correctness.

Q1. Au: Please check for empty boxes in text where special characters should be, and provide correct characters.

TABLE OF CONTENTS LISTING

The table of contents for the journal will list your paper exactly as it appears below:

Extended X-Ray Absorption Fine Structure and X-Ray Diffraction Studies of Mn-Doped PZN-PZT Ceramics
Athipong Ngamjarurojana, Laongnuan Srisombat, Rattikorn Yimnirun, and Supon Ananta

Ferroelectrics, 405:1–7, 2010

ISSN: 0015-0193 print / 1563-5112 online
DOI: 10.1080/00150193.2010.482888

Taylor & Francis
Taylor & Francis Group

Extended X-Ray Absorption Fine Structure and X-Ray Diffraction Studies of Mn-Doped PZN-PZT Ceramics

ATHIPONG NGAMJARUROJANA,[1,4]
LAONGNUAN SRISOMBAT,[2] RATTIKORN YIMNIRUN,[3]
AND SUPON ANANTA[1,*]

[1]Department of Physics and Materials Science, Faculty of Science, Chiang Mai University, Chiang Mai 50200, Thailand
[2]Department of Chemistry, Faculty of Science, Chiang Mai University, Chiang Mai 50200, Thailand
[3]School of Physics, Suranaree University of Technology, Nakhon Ratchasima 30000, Thailand
[4]ThEP Center, CHE, 328 Si Ayutthaya Road, Bangkok 10400, Thailand

In this work, the selected compositions of a combination between perovskite piezoelectric ceramics lead zinc niobate (PZN) and lead zirconate titanate (PZT), close to the morphotropic phase boundary (MPB) i.e. the 0.2PZN-0.8PZT, doped with MnO_2 concentrations of 0.0–0.9 wt% were fabricated by a simple solid-state reaction and a pressureless sintering techniques. X-ray diffraction (XRD) spectra from these materials reveal transformation of the tetragonal into the rhombohedral structure. The local structure of Mn was analyzed by mean of synchrotron extended X-ray absorption fine structure (EXAFS) measurements at the Mn K-edge. The correlation between the structural changes and the Mn content was analyzed and compared. The EXAFS analysis indicates that Mn ions should occupy the B-sites in PZN-PZT structure and plays a critical role for the hard ferroelectric behavior of the material.

Keywords Piezoceramics; perovskite; EXAFS; X-ray diffraction

1. Introduction

Lead-based complex perovskite piezoceramics with general formula $Pb(B',B'')O_3$ such as PZN, PZT and their solid-solutions close to the MPB are very attractive for sensor, transducer and actuator applications [1–3]. This is because of their low firing temperature and excellent piezoelectric properties. It has been widely proposed that these important properties strongly depend on the rotations and distortions of the BO_6 octahedra [1, 2]. Manganese oxide is one of the key effective dopants for lead-based perovskite piezoceramics to exhibit hard ferroelectric behavior [4–6]. Because of different valence of Mn and B-site ions, an enhancement in the Mn/B-site ions ratio may increase the vacancy concentration, forming acceptor-type defects and/or etc. In our previous work [7], the structure

Received August 23, 2009; in final form October 9, 2009.
*Corresponding author. E-mail: suponananta@yahoo.com

and electrical properties of MnO_2-doped 0.2PZN-0.8PZT compositions were investigated. It was found that with the addition of MnO_2, Curie temperature, the piezoelectric constant and electromechanical coupling factor were slightly decreased, but the mechanical quality factor was significantly enhanced. However, so far, the nature of the hard ferroelectric response and the site preference of Mn in these complex perovskite materials are still unclear [4–7]. Additionally, these previous investigation on Mn-doped PZT-based ceramics has also assumed that Mn ions sit in B-site [4–7]. Interestingly, so far, there has been no direct experimental determination of Mn-site in these materials. Thus, in this work, a combination of X-ray diffraction (XRD) and synchrotron extended X-ray absorption fine structure (EXAFS) experiments [8, 9], which is proven to be a powerful technique for resolving the local structure surrounding a particular (absorbing) atom, was performed on the Mn-doped PZN-PZT system in order to determine the local structure around Mn ions.

2. Experimental

The selected samples studied were fabricated according to the formula $0.2Pb(Zn_{1/3}Nb_{2/3})O_3$-$0.8Pb(Zr_{1/2}Ti_{1/2})O_3 + x$ wt% MnO_2, where $x = 0.0$ to 0.9 by a simple mixed-oxide method as detail described elsewhere [7]. Starting materials of PbO, ZnO, Nb_2O_5, ZrO_2, TiO_2, and MnO_2 with >99% purity were vibro-milled with zirconia media in isopropanal for 30 min. After drying, the powders were calcined at 900°C for 2 h. The calcined PZN-PZT powders were vibro-milled with MnO_2 additive and PVA binder for 30 min, pressed into pellets and fired at 500°C for 1 h to eliminate the PVA, followed by sintering with PbO-rich atmosphere inside sealed alumina crucible at 1200°C for 2 h [7]. Phase identification of the samples was performed by XRD and densities were measured by Archimedes method. The synchrotron EXAFS measurement was performed in the transmission mode at the X-ray absorption spectroscopy beamline (BL-8) of the Siam photon source (electron energy of 1.2 GeV), Synchrotron Light Research Institute (Public Organization), Thailand (Fig. 1). The spectra were collected at ambient temperature with a Ge(111) double crystal

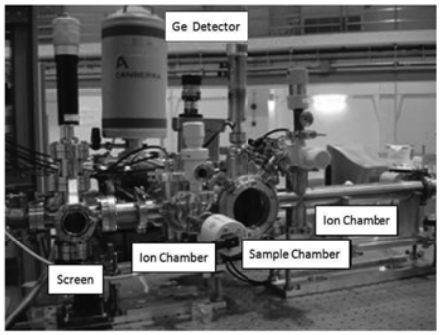

Figure 1. EXAF experimental set-up at BL8, SPS.

monochromator and recorded after performing an energy calibration. To increase the count rate, the ionization chamber was filled with Ar gas. The storage ring was running at an energy of 1.2 GeV with electron currents between 80 mA and 30 mA.

3. Results and Discussion

The XRD patterns of $0.2Pb(Zn_{1/3}Nb_{2/3})O_3$–$0.8Pb(Zr_{0.52}Ti_{0.48})O_3$ ceramics at different Mn concentrations are shown in Fig. 2. In general, the strongest reflections apparent in the majority of these XRD patterns indicate the formation of the pure perovskite phase for all compositions. It should be noted that no evidence of the pyrochlore-type compounds [10, 11] was found in this study, nor was there any indication of the unreacted precursors [12] being present. This is possibly due to uses of different processing methods. In those either works, a conventional ball-milling was employed, while the rapid vibro-milling used in this present study results in finer powders with apparently more reactivity, hence the pure perovskite phase is formed more easily. Furthermore, the effective suppression of PbO volatilazion commonly found for lead-based perovskite ceramics during high firing temperature [1, 2] was also achieved with the designed sample arrangement for the sintering scheme [7] The undoped PZN-PZT ceramics were characterized as tetragonal phase which is indicatedby the splitting of $(002)_T$ and $(200)_T$ peaks in the 2θ range from 43 to 45°, similar to the reported by Hou *et al.* [13] and Yang *et al.* [14]. It is noticed that a small amount of rhombohedral phase is also present with increasing Mn substitution with a complete transformation to rhombohedral phase (revealed by the single $(202)_R$ peak) when x reaches 0.5 wt%). This is similar to the circumstance of PZN (rhombohedral phase) addition on PZT system earlier reported by Lee *et al.* [11]. In addition, the effect of Mn on the shift of MPB toward the rhombohedral phase region in the similar system of Mn-doped PZT ceramics was also observed by Kim and Yoon [6]. It is believed that manganese ions are mainly incorporated into the lattice, but if the addition is above 0.5 wt%, manganese ions will accumulate at the grain boundaries [5]. It has been reported that manganese coexists mainly in the Mn^{2+} and Mn^{3+} states, which entered into the perovskite structure of BO_6 octahedron to substitute for the B-site ion (e.g. Ti^{4+} and Zr^{4+}).

The MPB composition range has believed to be quite narrow, but in practice the MPB has a wide range of compositions over which the tetragonal and rhombohedral phases coexist in ceramics. Since all properties take extreme values near MPB, the width of the MPB has been investigated by many workers and found to be related to the heterogeneous distribution of Zr^{4+} and Ti^{4+} cations on the B-site of perovskite lattice [5, 6]. By means of XRD, the co-existence of the two phases over a range of compositions around the MPB was demonstrated in this work. The smaller ionic radius of Mn^{4+} ion (0.053 nm) compared with that of the B-site ions (either Zn^{2+} (0.083 nm), Nb^{5+} (0.069 nm), Zr^{4+} (0.082 nm) or Ti^{4+} (0.064 nm) [1, 15] leads to the reductions in the lattice constants (and tetragonality) in Mn-doped PZN-PZT ceramics. However, the information on site preference of Mn in PZN-PZT perovskite structure cannot be retrieved directly from the XRD analysis alone. The EXAFS analysis was then employed to further study the local structure of Mn in the PZN-PZT-based lattice.

Figure 3 show the Mn K edge and Fourier transforms for the EXAFS spectra with possible bonding information identified and local structure of Mn-doped 0.2PZN-0.8PZT ceramics. The Fourier transform is a complex function of distance R, the amplitude of which is denoted by the real function $\rho(R)$. The position of peaks in $\rho(R)$ is related to bond distances between the Mn ion and neighboring ions while the height of each peak is proportional to the number of neighbors. The bond lengths and coordination numbers

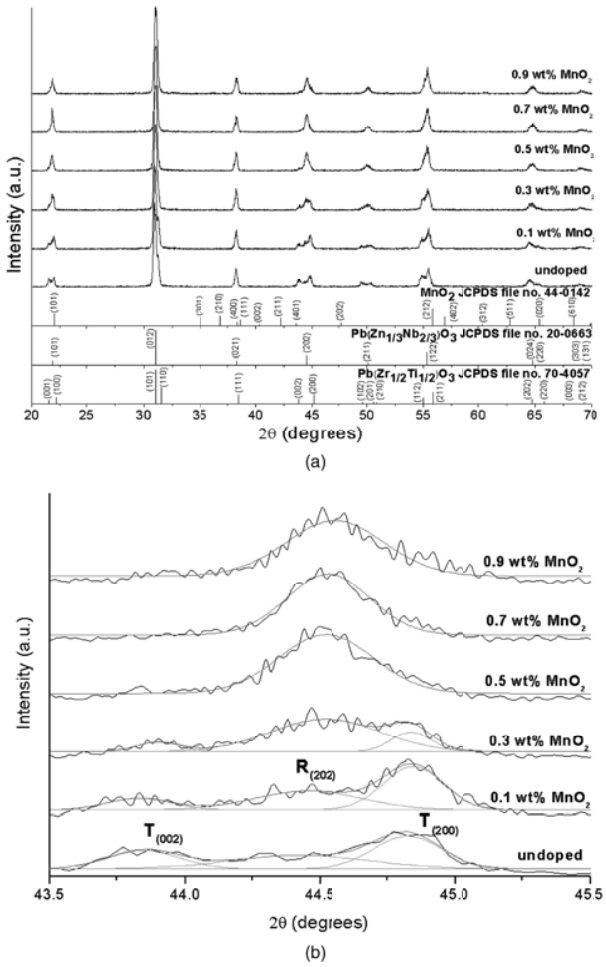

Figure 2. (a) XRD patterns of $0.2Pb(Zn_{1/3}Nb_{2/3})O_3$–$0.8Pb(Zr_{1/2}Ti_{1/2})O_3 + x$ wt% MnO_2, where $x =$ 0.0 to 0.9 and (b) enlarged XRD patterns in the $2\theta = 43$–46°. (See Color Plate XXX)

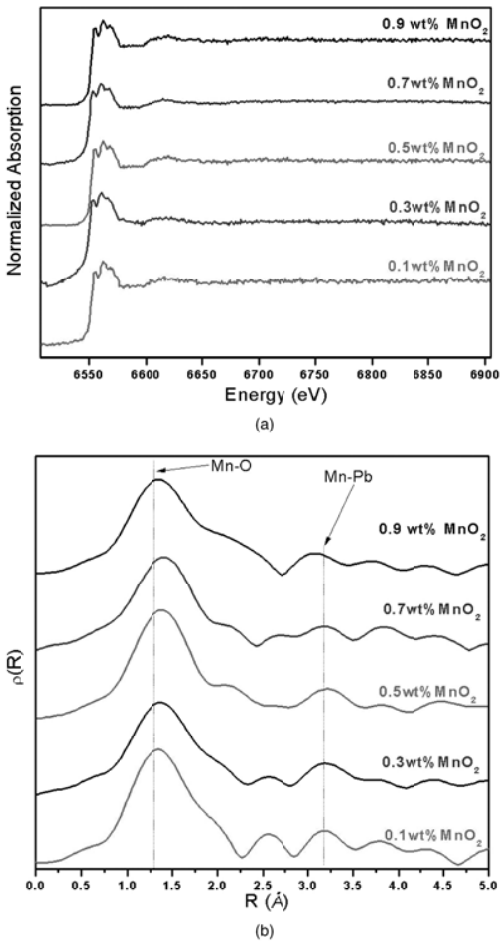

Figure 3. (a) Mn K edge spectra of MnO_2 doped 0.2FZN-0.8PZT ceramics, (b) Fourier transfoms of the EXAFS spectra for MnO_2 doped 0.2PZN-0.8PZT ceramics (peaks are designed with possible bonding) and (c) Possible local structure for Mn-doped 0.2PZN-0.8PZT ceramics. (See Color Plate XXX)

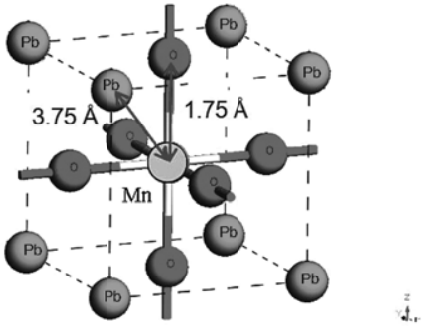

(c)

Figure 3. (Continued)

cannot, however, be read directly from $\rho(R)$. In order to determine the bond lengths and coordination numbers, the k-dependent amplitude and phase corrections must be made to the EXAFS signal. For example, prior to the phase correction, the peaks in $\rho(R)$ are basically smaller than the corresponding bond lengths by ~0.5 Å [9]. Interestingly, the location of Mn within PZN-PZT unit cell can be resolved without making phase and amplitude corrections. As shown in Fig. 3, by simply comparing the raw Fourier transform for different Mn contents (0.1–0.9 wt%), there is no observable change in peak positions, particularly for the first main peak. The coincidence of the main peaks is evidence that no change in the location of the majority of Mn ions occurs with increasing Mn concentration. Furthermore, the location of Mn appears to be unaffected by the presence of 0.9 wt% MnO_2. It should be noted that a similar Fourier transform of EXAFS spectra for Mn doped PZN-PZT in this study, Mn doped PZT reported by Cherdhirunkorn *et al.* [9] and PZN, PZT perovksite established by Chen [16] is observed. The results indicate the site of Mn atom at B(Zn,Nb,Zr,Ti)-site in the PZN-PZT unit cell. Since the peak position indicates the bond distance between Mn and its neighbors or the location of Mn within the PZN-PZT unit cell, the unit cell of Mn-doped PZN-PZT can be extracted from the peak positions in the Fourier transform of EXAFS spectra shown in Fig. 3. According to the simulation EXAFS for Mn-doped PZT established by Cherdhirunkorn *et al.* [9], similar information can be extracted from the Fourier transforms of the EXAFS spectra from Mn-doped PZN-PZT observed in this work. It is very interesting to observe similar EXAFS signatures between the Mn-B-site curve where the first main peak occurring at ~1.25 Å (due to the six nearest oxygen atoms), while the second peak at ~3.2 Å is attributed to the nearest Pb atoms. Furthermore by comparing the results shown in Fig. 3 and Ref. [16], it is evident that the peaks are well consistent with a simulation of EXAFS that assumes Mn occupies the B-site but the minority A-site occupation cannot be ruled out.

4. Conclusions

A combination of X-ray diffraction and synchrotron extended X-ray absorption fine structure experiments is performed on Mn-doped $0.2Pb(Zn_{1/3}Nb_{2/3})O_3$–$0.8Pb(Zr_{1/2}Ti_{1/2})O_3$. The transformation of the tetragonal into the rhombohedral structure with increasing Mn content was revealed by XRD technique. The EXAFS analysis indicates that Mn ions should occupy the B(Zn, Nb, Zr, Ti)-sites in PZN-PZT structure and plays a critical role for the hard ferroelectric behavior of the materials.

Acknowledgment

This work was supported by the Synchrotron Light Research Institute (Public Organization), Thailand (GRANT 1-2551/PS02) and the Faculty of Science, Chiang Mai University.

References

1. A. J. Moulson and J. M. Herbert, *Electroceramics*. New York: Wiley-Interscience (2003).
2. Y. Xu, *Ferroelectric Materials and Their Applications*. Los Angeles: North Holland (1991).
3. K. Uchino, *Ferroelectric Devices*. New York: Marcel Dekker (2000).
4. Y. Hou, M. Zhu, F. Gao, H. Wang, B. Wang, H. Yan, and C. Tian, Effect of MnO_2 addition on the structure and electrical properties of $Pb(Zn_{1/3}Nb_{2/3})_{0.20}(Zr_{0.50}Ti_{0.50})_{0.80}O_3$ ceramics. *J. Am. Ceram Soc.* **87**, 847–850 (2004).
5. L. X. He and C. E. Li, Effects of addition of MnO on piezoelectric propertis of lead zirconate titanate. *J. Mater. Sci.* **35**, 2477–2480 (2000).
6. J. S. Kim and K. H. Yoon, Physical and electrical properties of MnO_2-doped $Pb(Zr_xTi_{1-x})O_3$ Ceramics. *J. Mater. Sci.* **29**, 809–815 (1994).
7. A. Ngamjarurojana and S. Ananta, Effect of MnO_2 addition on dielectric, piezoelectric and ferroelectric properties of $0.2Pb(Zn_{1/3}Nb_{2/3})O_3$–$0.8Pb(Zr_{1/2}Ti_{1/2})O_3$ ceramics. *Chiang Mai. J. Sci.* **36**, 59–68 (2009).
8. E. R. Kipkoech, F. Azough, R. Freer, and J. F. Mosselmans, Extended x-ray absorption fine structure analysis of $(Cd,Nd)(Ti,Al)O_3$ perovskite ceramics used in cellular base stations. *Acta Mater.* **54**, 2305–2309 (2006).
9. B. Cherdhirunkorn, M. F. Smith, S. Limpijumnorg, and D. A. Hall, EXAFS study on the site preference of Mn in perovskie structure of PZT ceramics. *Ceram Inter.* **34**, 727–729 (2008).
10. S. Zhao, H. Wu, and Q. Sun, Study on PSN-PZN-PZT quaternary piezoelectric ceramics near the morphotropic phase boundary. *Mater. Sci. Eng B* **123**, 203–210 (2005).
11. S. H. Lee, C. B. Yoon, S. M. Lee, and H. E. Kim, Reaction sintering of lead zinc nibate-lead zirconate titanate ceramics. *J. Eur. Ceram Soc.* **26**, 111–115 (2006).
12. D. H. Suh, N. K. Kim, and J. H. Kim, Crystallographic and dielectric studies on $Pb(Zn_{1/3}Ta_{2/3})O_3$-substituted $Pb[(Zn_{1/3}Nb_{2/3}),Ti]O_3$ system. *Mater. Lett.* **50**, 6–11 (2001).
13. Y. Hou, M. Zhu, H. Wang, B. Wang, H. Yan, and C. Tian, Effects of CuO addition on the structure and electrical properties of low temperature sintered $Pb((Zn_{1/3}Nb_{2/3})_{0.20}(Zr_{0.50}Ti_{0.50})_{0.80})O_3$ ceramics. *Mater. Sci. Eng. B* **110**, 27–31 (2004).
14. Z. Yang, H. Li, X. Zong, and Y. Chang, Structure and electrical properties of PZT-PMS-PZN piezoelectric ceramics. *J. Eur. Ceram Soc.* **26**, 3197–3202 (2006).
15. R. D. Shannon and C. T. Prewitt, Effective ionic radii in oxides and fluorites. *Acta Crystallogr. B* **25**, 925–946 (1969).
16. I. W. Chen, Structural origin of relaxor ferroelectrics-revisited. *J. Phys. Chem. Solid.* **61**, 197–208 (2000).